ARTICLE

Vertically Aligned Boron Nitride Nanosheets: Chemical Vapor Synthesis, Ultraviolet Light Emission, and Superhydrophobicity

Jie Yu,[†,*] Li Qin,[†] Yufeng Hao,[†] Shengyong Kuang,[†] Xuedong Bai,[‡] Yat-Ming Chong,[§] Wenjun Zhang,[§] and Enge Wang[‡]

[†]Department of Materials Science and Engineering, Shenzhen Graduate School, Harbin Institute of Technology, Xili, Shenzhen 518055, China, [‡]Beijing National Laboratory for Condensed Matter Physics, Institute of Physics, Chinese Academy of Sciences, Beijing 100080, China, and [§]Center of Super-Diamond and Advanced Films (COSDAF) and Department of Physics and Materials Science, City University of Hong Kong, Kowloon, Hong Kong SAR, China

ABSTRACT Boron nitride (BN) is a promising semiconductor with a wide band gap (~6 eV). Here, we report the synthesis of vertically aligned BN nanosheets (BNNSs) on silicon substrates by microwave plasma chemical vapor deposition from a gas mixture of BF_3—N_2—H_2. The size, shape, thickness, density, and alignment of the BNNSs were well-controlled by appropriately changing the growth conditions. With changing the gas flow rates of BF_3 and H_2 as well as their ratio, the BNNSs evolve from three-dimensional with branches to two-dimensional with smooth surface and their thickness changes from 20 to below 5 nm. The growth of the BNNSs rather than uniform granular films is attributed to the particular chemical properties of the gas system, mainly the strong etching effect of fluorine. The alignment of the BNNSs is possibly induced by the electrical field generated in plasma sheath. Strong UV light emission with a broad band ranging from 200 to 400 nm and superhydrophobicity with contact angles over 150° were obtained for the vertically aligned BNNSs. The present BNNSs possess the properties complementary to carbon nanosheets such as intrinsically semiconducting, high temperature stability, and high chemical inertness and may find applications in ultraviolet nanoelectronics, catalyst supports, electron field emission, and self-cleaning coatings, *etc.*, especially those working at high temperature and in harsh environments.

KEYWORDS: boron nitride nanosheets · alignment · chemical vapor deposition · cathodoluminescence · superhydrophobicity

Two-dimensional (2D) nanostructures have attracted a great deal of attention due to their exceptional properties and potential applications since the discovery of graphene.[1] The previous research on nanomaterials is mainly focused on zero-dimensional (0D) and one-dimensional (1D) nanostructures such as fullerenes (C_{60}) and carbon nanotubes, while the 2D nanomaterials were apparently neglected maybe due to the prediction that atomically thin 2D crystals are not stable in ambient environment. Graphene has been regarded as a rising star in materials science due to the high promise in applications of electronic devices based on its unique properties such as high room-temperature mobility.[1] Besides the single layer graphene, multilayer carbon nanosheets (nanowalls) generally with thickness below 20 nm also attract much attention mainly because of their distinctive shape, high surface-to-volume ratio, and sharp open edges.[2−5] To date, different applications such as composite fillers for enhancing thermal conductivity,[6] supports for functional nanoparticles,[7] electrodes of Li-ion batteries,[8] electron field emitters,[3] and biosensors[5] have been demonstrated for the carbon nanosheets, showing the importance of the 2D nanomaterials.

With the extensive research on carbon nanomaterials, great interest in boron nitride (BN) arises naturally owing to their structural similarity. Similar to carbon, BN also exists in the forms of sp^2-bonded rhombohedral and hexagonal BN (hBN) or sp^3-bonded wurtzite and cubic BN (cBN), among which hBN and cBN are the most common forms. The hBN is isostructural to graphite and able to bend and curl to form fullerene-like structures[9,10] and nanotubes.[11] The research on BN nanomaterials is mainly driven by the fact that BN is a semiconductor with a wide band gap near 6 eV,[12] in contrast to the semimetallic nature of graphite, and possesses much higher chemical and thermal stability than carbon,[11,13,14] which provide attractive properties complementary to their carbon counterparts. Recent report has demonstrated that BN is of high promise in applications of ultraviolet (UV) light emission devices.[12] As the main member of BN nanomaterials, BN nanotubes (BNNTs) have been synthesized and investigated considerably and found to have many promising

*Address correspondence to jyu@hitsz.edu.cn.

Received for review September 10, 2009 and accepted December 22, 2009.

Published online January 4, 2010. 10.1021/nn901204c

© 2010 American Chemical Society

applications such as polymeric composites, gas adsorption, electrical nanoinsulators, electron field emission, and ultraviolet nanoelectronics.[11,15−22] Interestingly, theoretical calculations have predicted that BNNTs are excellent piezoelectrics,[23] and superlattice or isolated CNT/BNNT junctions could produce itinerant ferromagnetism and spin polarization.[24,25] It is thus considered that 2D BN nanostructures may have many interesting properties and find innovative applications in various areas. Surprisingly, it has been demonstrated that the BN nanoribbons with zigzag edges can behave as metals, thus exhibiting excellent electron field emission properties.[26] Recently, mono- and few-atomic-layer BN sheets have been prepared by mechanical cleavage and chemical exfoliation from bulk BN crystals.[27,28] However, synthesis of BN nanosheets (BNNSs) with controlled structure and orientation directly on substrates has not been reported so far.

Herein, we report the synthesis of vertically aligned 2D BNNSs directly on silicon substrates from gas mixtures of $BF_3-N_2-H_2$ by the widely used microwave plasma chemical vapor deposition (MPCVD) technique. The processes of controlling the size, shape, density, and orientation of the BNNSs were well-established. Interesting properties of UV light emission and superhydrophobicity were obtained for the BNNS films, indicating their application potential for nanoelectronics and self-cleaning coatings.

RESULTS AND DISCUSSION

Figure 1 shows the scanning electron microscopy (SEM) images of the samples grown for 1 h at different BF_3 and H_2 flow rates. Unexpectedly, we obtained the BNNSs rather than the conventional granular films, although no catalysts were used. These BNNSs are generally well-separated with a bending and crumpling morphology and tend to be vertically aligned though we did not use templates or bias. We found that the growth of the BNNSs is strongly dependent on the gas flow rates of H_2 and BF_3 as well as their ratio. If not introducing H_2, no deposits were obtained at any BF_3 flow rates (R_{BF_3}). Nevertheless, if R_{BF_3} was too low, the nanosheet formation could not occur even with introduction of H_2. The minimal H_2 flow rate (R_{H_2}) required for the nanosheet formation decreases with increasing R_{BF_3} in the parameter range applied in this study. At the R_{BF_3} of 5, 3, and 2 sccm, the BNNSs start to grow at the R_{H_2} of 10, 10, and 30 sccm (Figure 1), respectively. When R_{BF_3} decreases to 1 sccm, the growth of the BNNSs was not observed at all R_{H_2} applied in this work. The structure of the BNNSs changes greatly with changing R_{BF_3}. Interestingly, at the R_{BF_3} of 5 sccm, the BNNSs are branching; that is, subnanosheets grow on the surface of the main nanosheets, forming three-dimensional nanostructures (Figure 1a). The length of the main nanosheets is in the range of 1.2−2.9 μm, and that of the subnanosheets is 80−600 nm. We consider that the branching BNNSs have the advantage of preventing conglomeration and thus are able to preserve their high surface area. The branching phenomenon of the BNNSs decreases greatly with decreasing R_{BF_3} to 3 sccm (Figure 1b), and the smooth BNNSs without branches were obtained when R_{BF_3} was decreased to 2 sccm (Figure 1c). The size of the BNNSs decreases markedly with decreasing the R_{BF_3}, and the length of the BNNSs prepared at the R_{BF_3} of 3 and 2 sccm are 0.5−1.6 and 0.28−0.67 μm, respectively (Figure 1). It is also noted that the BNNSs prepared at the R_{BF_3} of 2 sccm is sparser and better separated from each other than that prepared at the R_{BF_3} of 3

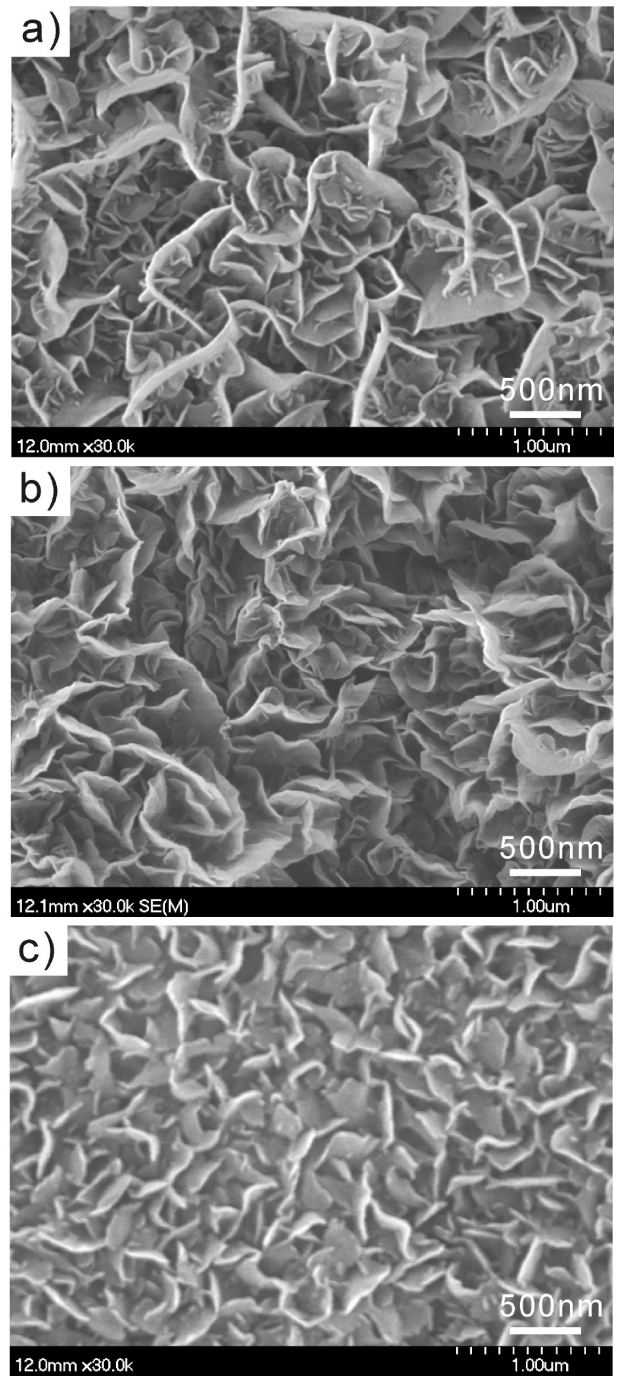

Figure 1. SEM images of the BNNSs grown for 60 min at different R_{BF_3}/R_{H_2} (sccm): (a) 5/10, (b) 3/10, (c) 2/30.

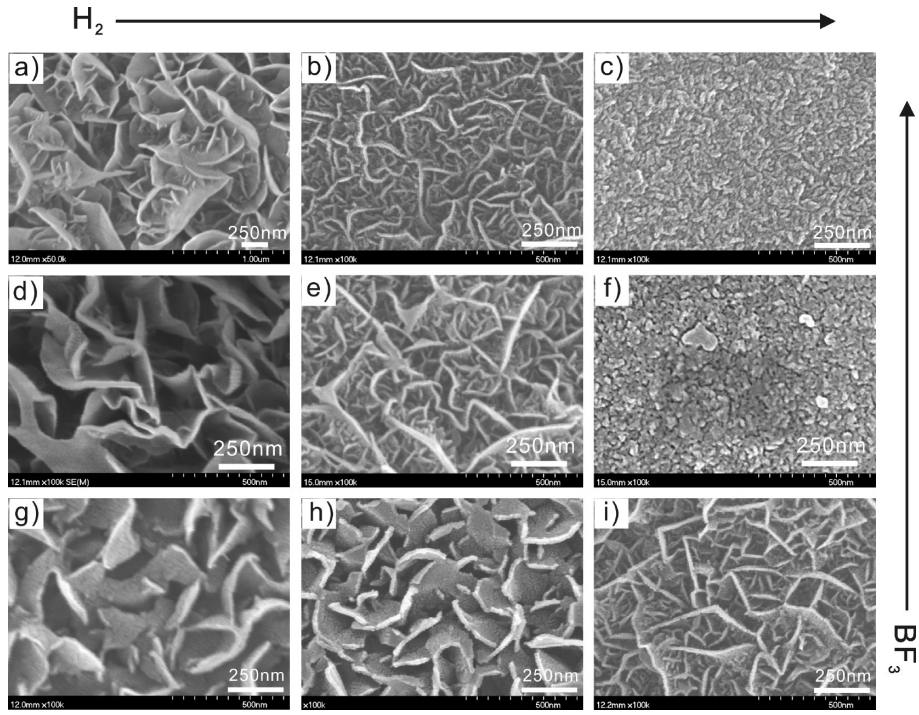

Figure 2. SEM images of the BNNSs grown at different R_{H_2}/R_{BF_3} (sccm): (a) 10/5, (b) 25/5, (c) 40/5, (d) 10/3, (e) 60/3, (f) 160/3, (g) 30/2, (h) 40/2, (i) 100/2.

and 5 sccm (Figure 1; also see Figure 2). Due to the edge bending of the BNNSs, it is difficult to accurately determine their thickness from the SEM images. For most of the nanosheets, the thickness could be roughly measured to be below 20 nm.

The effects of R_{H_2} on the growth of the BNNSs were investigated by keeping R_{BF_3} constant, as shown in Figure 2. It is clearly observed that the growth of the BNNSs is greatly dependent on R_{H_2} at constant R_{BF_3} and tend to occur at lower R_{H_2} and R_{BF_3}. With increasing R_{H_2} at constant R_{BF_3} the nanosheets become thicker, coarser, and more branching, and only granular films were deposited finally. We found that the growth rates of the BNNSs were much lower than that reported for the carbon nanosheets (nanowalls), which could be observed only after several minutes of deposition.[2−4] In this study, the BNNSs were grown for 30, 60, and 180 min, but for the 30 min deposition, no BNNSs was observed. Figure 3 shows a typical SEM image of the BNNSs grown for 180 min at the R_{BF_3}/R_{H_2} of 3/10 sccm. It is indicated that the BNNSs become interconnected with the alignment improved obviously, forming the morphology similar to the reported carbon nanowalls.[2−5]

Figure 4 shows the transmission electron microscopy (TEM) images of the BNNSs prepared at the R_{BF_3}/R_{H_2} of 5/10 sccm and the corresponding electron energy loss spectrum (EELS). From Figure 4a, it is clearly observed that the BNNSs are bending and scrolling with tapered edge morphology, similar to that reported for the carbon nanosheets.[5] Bending and scrolling is intrinsic for the 2D nanostructures, which have been repeatedly reported. The dark parts are generally the cross sections of the BNNSs folded back. Figure 4b is the high resolution TEM (HRTEM) image showing the cross section of the BNNS marked with rectangle A, the thickness of which was measured to be 15.9 nm. The inset is the enlarged image of the area in rectangle C, where highly ordered lattice fringes can be clearly observed, indicating that the BNNSs are well-crystallized. The average spacing between adjacent fringes was measured to be 0.341 nm, manifesting that the lattice fringes are (002) crystal planes of hBN. By measurements on many nanosheets, we found that the interplane spacing of (002) is mostly in the range of 0.333−0.355 nm. We observed that

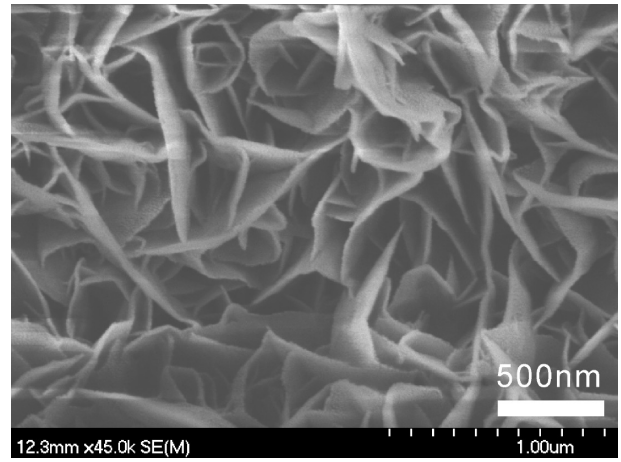

Figure 3. Typical SEM image of the BNNSs grown for 180 min at the R_{BF_3}/R_{H_2} of 3/10 sccm.

the crystallity is not uniform for individual BNNSs. Generally, the hexagonal layers in the inner part are straight and in good parallel to each other, but bending, distortion, and discontinuities were frequently observed for the outer layers. By approaching the nanosheet edges, the thickness of the BNNSs decreases gradually, forming the knife-edge or cone-like structures and leaving many open layers on the surface (Figure 4c). These open layers are attractive for applications of hydrogen storage, electron field emission, sensors, and catalyst supports due to their high reaction activity.

Electron energy loss spectra (EELS) were recorded during TEM measurements for determining the stoichiometry and chemical states of the BNNSs. The typical EELS spectrum exhibits two distinct absorption features starting at 188 and 401 eV (Figure 4d), corresponding to the known K-shell ionization edges of boron (B−K) and nitrogen (N−K), respectively. The sharp π* peaks on the left side of the B−K and N−K edges and the shapes of the σ* bands on the right side are typical of the sp^2-bonded layered BN.[17−19] Only B−K and N−K edges were observed with the B/N ratio calculated to be about 1.0. EELS measurements on many BNNSs present similar results, indicating that the obtained BNNSs are pure boron nitride with hexagonal layered structure. From the TEM measurements, we also found that the thickness of the BNNFs is dependent on R_{BF_3}/R_{H_2}. Figure 5 shows the TEM images of the BNNSs grown at the R_{BF_3}/R_{H_2} of 2/30 sccm, where the translucent nature of the BNNSs can be observed, suggesting that the BNNSs are very thin (Figure 5a). From the turned-up edges of the BNNSs, it was found that many nanosheets are below 5 nm in thickness with about 10 atomic layers (Figure 5b). Obviously, the thickness of the BNNSs was decreased considerably by changing the R_{BF_3}/R_{H_2} from 5/10 to 2/30 sccm.

Raman spectroscopy and Fourier transform infrared spectroscopy (FTIR) were also used to characterize the BNNSs. Figure 6a shows the typical Raman spectrum of the BNNSs, where an intense peak appears at 1366 cm^{-1}, attributed to the high frequency intralayer E_{2g} vibration mode of hBN.[29−32] Raman spectroscopy has been widely used to identify the structure of BN materials as a sensitive tool. Crystalline hBN has D_{6h}^4 space group symmetry and the symmetry transformations of the zone-center optical phonons are given by $\Gamma = 2E_{2g} + 2B_{1g} + A_{2u} + E_{1u}$. Of these, the E_{2g} modes are Raman-active, the A_{2u} and E_{1u} modes are IR-active, and the B_{1g} modes are optically inactive.[29−31] Both of the two Raman-active E_{2g} modes are due to in-plane atomic displacements. Of them, the low frequency mode is characterized by whole planes sliding against each other, and the high frequency mode is due to B and N atoms moving against each other within a plane. The low frequency mode is at 49−52.5 cm^{-1},[30,31,33] but it less observed maybe mainly because of its low intensity and high Rayleigh background. In the present

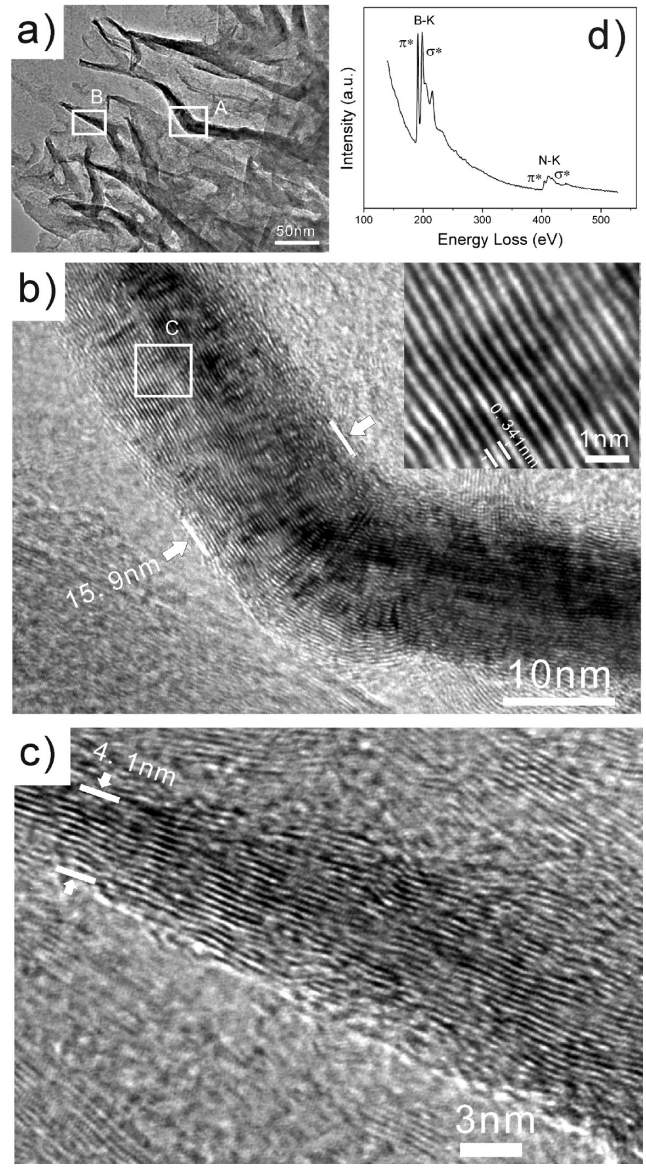

Figure 4. TEM images and EELS spectrum of the BNNSs prepared at the R_{BF_3}/R_{H_2} of 5/10 sccm. (a) Low magnification TEM image. (b) HR-TEM image showing the area in rectangle A (the inset is the enlarged image of the area in rectangle C). (c) HRTEM image showing the area of rectangle B. (d) EELS spectrum.

study, the low frequency mode was not detected due to the detection limit of our Raman system. The crystallinity of BN materials can be evaluated by positions and full width at half-maximun (fwhm) of the Raman peaks. Nemanich *et al.* have shown that both position and fwhm for the high frequency E_{2g} mode vary inversely with crystallite size (base-plane dimension).[30] The high frequency E_{2g} mode has been measured for different BN materials such as single-crystal BN (1366 cm^{-1}),[33] highly ordered pyrolytic BN (1366−1367 cm^{-1}),[30,31] and polycrystalline BN (1367−1374 cm^{-1}).[30] For single-walled BNNTs, an asymmetric and broadened peak due to a composite signal of the tangential A_g and longitudinal E_{2g} modes is located at 1370 cm^{-1}, which is intrinsic for the single-walled BNNTs.[34] The Ra-

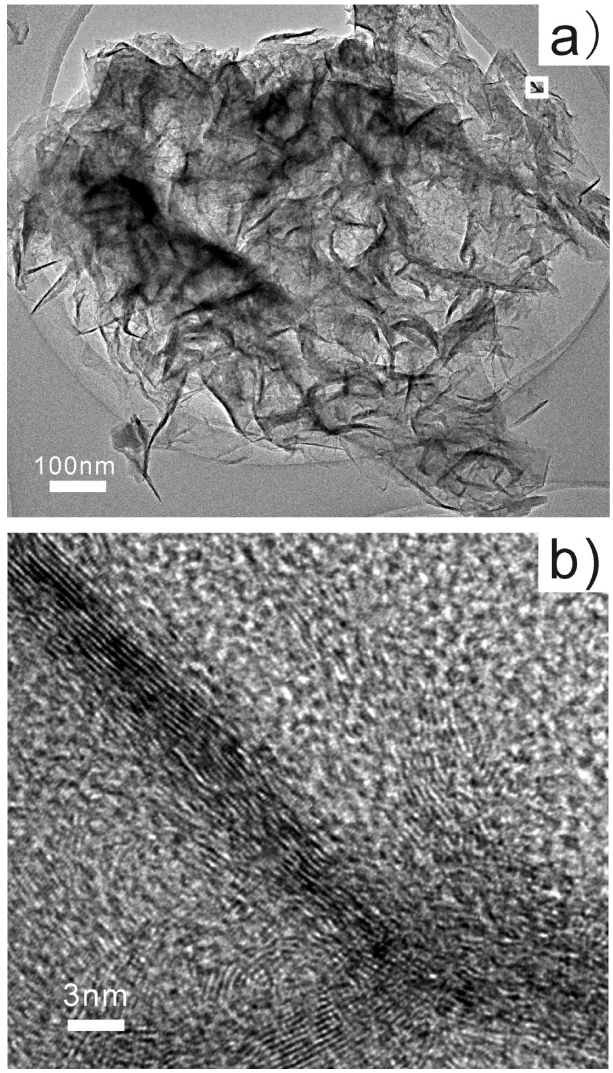

Figure 5. TEM images of the BNNSs grown at the R_{BF_3}/R_{H_2} of 2/30 sccm. (a) Low magnification image. (b) HRTEM image showing the cross section of the BNNS taken from the area marked with the rectangle in panel (a).

man spectrum of the BNNSs shows no new features and is similar to that of bulk hBN due to their multilayer structure. The fwhm of the E_{2g} mode is about 19 cm^{-1} for the present BNNSs, which is larger than that of high temperature (~1900 °C) CVD synthesized pyrolytic BN (~16 cm^{-1})[31,35] and high temperature (1600−1700 °C) synthesized BNNTs (13 cm^{-1}),[32,36] but smaller than that of the pyrolytic BN measured by Geick *et al.* (~30 cm^{-1})[29] and the BNNTs (27 cm^{-1}) synthesized at lower temperature (1200 °C).[37] This indicates that the BNNSs are relatively well-crystallized, although the growth temperature is low (~800 °C), which may be a result of the etching effect of fluorine in the gas phase as we will discuss later. Figure 6b is a typical Fourier transform infrared (FTIR) spectrum of the BNNSs. In the spectrum, we observed one sharp absorption peak at 811 cm^{-1} and one broad absorption band with the bottom in the range of 1350−1520 cm^{-1}, which we ascribed to the A_{2u} (B−N−B bending vibration mode parallel to the *c*-axis) and E_{1u} (B−N stretching vibration mode perpendicular to the *c*-axis) modes of hBN,[13,29,38−40] respectively. Because the film is too thick, the tramsmittance decreased to zero for the E_{1u} mode. The FTIR spectra of different BN materials have been reported by many researchers. The A_{2u} and E_{1u} modes are located at 811 and 1377 cm^{-1} for polycrystalline hBN[40] and 818 and 1367 cm^{-1} for BN hollow nanoribbons.[39] For multiwalled BNNTs prepared at 1500[40] and 1700 °C,[36] the A_{2u} and E_{1u} modes are at 800 and 1372 cm^{-1} and 820 and 1366 cm^{-1}, respectively, with obvious peak splitting between the transverse and longitudinal optical modes under normal incidence of IR light. The present FTIR spectrum of the BNNSs is similar to that of the polycrystalline hBN and BN hollow nanoribbons, confirming their relatively good crystallinity.

Many researchers have reported the synthesis of hBN films by CVD from various source gases such as B_2H_6,[41] BCl_3,[42] BBr_3,[43] and $BH_3NH(CH_3)_2$.[44] However, no one observed the growth of the BNNSs in these studies. We consider that the well-controlled growth of the BNNSs in the present study is mainly due to the particular chemical properties of the gas system containing H and F elements. It has been demonstrated that fluorine, mainly F atoms generated in plasma, is an effective etchant of hBN.[45−47] By utilizing the preferential etching effect of fluorine on hBN, we have successfully synthesized high quality cBN films from the gas system of $BF_3-N_2-H_2-Ar$.[48,49] Both thermodynamic calculation[50] and experimental results[45,46] show that no solid BN forms in the $Ar-N_2-BF_3$ system due to the strong etching of F atoms. This is the reason that we could not obtain the BN deposits without introducing H_2. With introducing H_2, the etching effect of F is balanced by forming stable HF molecules more or less depending on the R_{H_2}/R_{BF_3} ratio, resulting in the deposition of solid BN.[45−47] The R_{H_2}/R_{BF_3} ratio controls the equilibrium between film formation and etching and thus controls the production rate of solid BN from the gas phase. At appropriately low R_{H_2}/R_{BF_3} ratio, the BN nuclei formed on the surfaces of the growing nanosheets will be etched off quickly by F atoms owing to the weak van der Waals force between them while the growing species reaching the nanosheet edges covalently bond with the edge atoms to form stable B−N bonds with much higher resistance to F etching, which causes the nanosheets to grow higher and longer rather than thicker. The branching and thickening of the BNNSs with increasing the R_{H_2}/R_{BF_3} ratio is caused by the corresponding decrease of F etching due to HF formation. With increasing the R_{H_2}/R_{BF_3} ratio high enough, the etching effect of fluorine vanishes because the F atoms in the plasma disappear due to forming HF, as indicated in ref 47. This leads to nearly equiaxial growth of hBN cyrstals and deposition of granular films. Because the growing atoms of B are from BF_3, the growth rate of solid BN increases with increasing R_{BF_3} at appropriate R_{H_2}/R_{BF_3} ratios,

and therefore, no BNNSs grow at too low R_{BF_3}. Vertical alignment of the BNNSs is most likely induced by the electrical field generated in the plasma sheath, according to the previous literature.[51] We have previously used the electrical field to induce alignment of boron carbonitride nanotubes successfully.[52,53] The effects of electrical field on inducing alignment of carbon nanotubes and carbon nanosheets have also been observed.[4,54,55] The aligned growth of hBN with (002) basal planes perpendicular to substrates was frequently observed as the intermediate layers in growing cBN films in the presence of plasma or ion bombardment,[51] which was generally explained to be caused by the ion-induced compressive stress. By the above mechanism, the growth behavior of the BNNSs can be well-understood.

Due to the prospective UV applications of BN materials, cathodoluminescence (CL) spectra were measured for the BNNSs. Figure 7a is a typical CL spectrum of the BNNSs, which exhibits a broad emission band centered around 265 nm (4.677 eV) in the range of 200−400 nm (6.198−3.099 eV). Some emission peaks have been reported and identified in this range, such as that at 215 nm from free exciton,[12] 220 and 227 nm from bound exciton,[12,56] and 300−400 nm from vacancies or residual impurities such as oxygen and carbon.[12,39,57,58] The present band should be ascribed to the superposition of the above-reported emissions. As shown in Figure 4, the inner part of the BNNS is highly crystallized. It is thus reasonable to ascribe the near-band-edge emission to the highly crystallized BN layers in the inner parts of the BNNSs. We consider that the presence of a great deal of open edges of the vertically aligned BNNSs, which are exposed to the irradiating electron beams, contribute greatly to the continuum of the emission band. The sharp features on the top of the emission band is likely related to the participation of phonons. The strong light emission up to 200 nm suggests that the BNNSs are of high promise for UV applications. For comparison, the typical CL spectrum of the granular BN films (as shown in Figure 2c,f) is shown in Figure 7b, where a broad emission band in the range of 260−520 nm centered around 360 nm is observed. Comparing with the CL spectrum of the BNNSs (Figure 7a), the CL emission band of the granular films broadens and shifts toward large wavelength. This band is obviously from defects without the near-band-edge emission. This is because the BNNSs are better crystallized than the granular films due to the enhanced etching effect of fluorine at lower R_{H_2}/R_{BF_3} ratio.

Wetting properties of water on the BNNS films were also measured due to their distinctive rough morphology with nanoscale features, which is generally able to generate superhydrophobicity as reported.[59] Figure 8a shows the shape of a water droplet on a BNNS film, the contact angle (CA) here is about 155°, indicating that the BNNF films are superhydrophobic. As is well-known, the hydrophobic properties of any surface can be greatly enhanced by introducing micro- and nanoroughness.[59] We

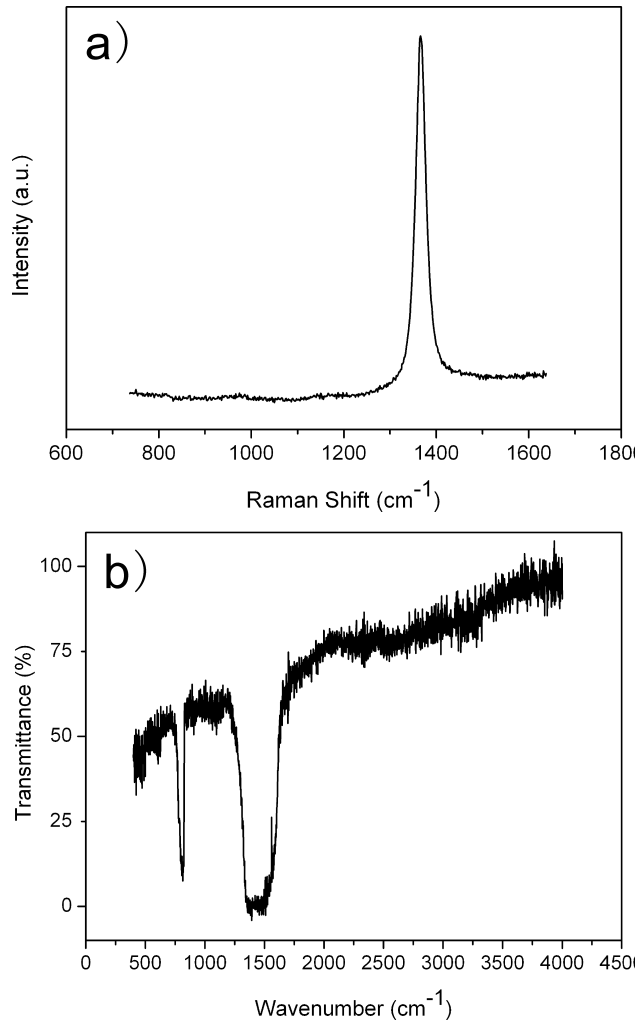

Figure 6. Typical Raman (a) and FTIR (b) spectra of the BNNSs.

here ascribe the superhydrophobicity of the BNNS film to its nanoscale rough surface. As a comparison, the shape of a water droplet on a common granular film (with morphology similar to Figure 2c,f) is shown in Figure 8b, where the CA is only about 40°. This confirms that the superhydrophobicity of the BNNS films is due to their nanoscale rough morphology. Recently, superhydrophobic materials have received much attention due to their important applications from self-cleaning surface to microfluidic devices. So far, most of the superhydrophobic surfaces were prepared by using organic materials,[59,60] which are generally fragile at high temperature and in harsh environments. Inorganic nanomaterials such as carbon nanotubes,[61] BNNTs,[62] and TiO_2 nanorods[63] have been used to prepare the superhydrophobic coatings. The present BNNS films with superhydrophobicity have the advantages of high chemical inertness, high temperature stability, and transparency (or white) as well as catalyst-free growth and enhanced bonding strength.

In order to further investigate the edge effects of the BNNSs, we measured the electron field emission properties of the BNNS films by the method we described previously.[64] It was found that the field emission of the BNNS

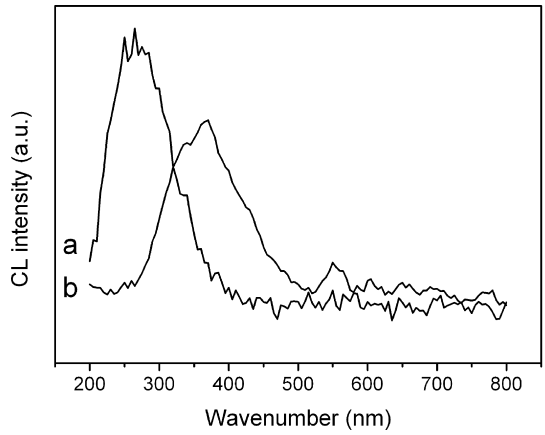

Figure 7. Typical CL spectra of the BNNSs (a) and granular films (b).

films is strongly dependent on their thickness. No electron emission was observed for the thicker samples with a thickness larger than 3 μm. This is reasonable because the pure BN is extremely insulating. In some of the thinner samples with a thickness of 1−2 μm, we observed electron emission at very high electrical field. In a typical case, the obvious electron emission was observed at 44.4 V/μm (turn-on field) with a current density at 0.072 μA/cm^2, and the current density increases to 250 μA/cm^2 at 74 V/μm. The present turn-on field is higher than that reported for the pure BN films.[65,66] However, the reported field emission is from very thin BN films with the turn-on field at 8.3, 15.2, and more than 20 V/μm for the film thickness of 7−8, 70, and 300 nm.[65,66] Compared to these BN films, the present BNNS films are much thicker. In addition, the present BNNSs are well-crystallized as indicated by the Raman spectra, CL, TEM, and SEM images, while the above-reported BN films are nanocrystalline or amorphous.[66] Therefore, we consider that the larger thickness and high crystallinity account for the high turn-on field or no electron emission for our BNNS films. Although, at high electrical field, it is surprising that the extremely insulating and thick BNNS films can pass electrons. However, it has been reported that the turn-on field from the BN ribbons can be as low as 1−1.3 V/μm at a high current density of 10 μA/cm^2, which was attributed to the presence of the metallic zigzag edges. In this work, the edge structure of the BNNSs was characterized by HRTEM and electron diffraction in an attempt to determine if the metallic zigzag edges are present in our samples. Unfortunately, we failed to determine the edge structure mainly because the BNNSs are multilayer and misorientation exists between the atomic layers, which were demonstrated by the distorted diffraction spots (not shown). Nevertheless, the electron field emission from the well-crystallized and very thick BNNS films is very likely caused by the edge effects of the nanosheets and the possible presence of some metallic edges as reported by Terrones *et al.*[26] It is expected that the electron field emission properties of the BNNS films can be greatly improved by reducing the film thickness, doping,[65] or making composite films with conductive materials. Due to the importance of the single-layer 2D materials, it is necessary to further decrease the layer numbers of the BNNSs and synthesize single-layer BN sheets. We have demonstrated that the thickness of the BNNSs can be effectively controlled by the flow rate ratio of R_{H_2}/R_{BF_3}. So it is possible to synthesize thinner or single-layer BN sheets by appropriately decreasing the R_{H_2}/R_{BF_3} ratio, that is, enhancing the etching effect of fluorine. By using the methods reported for preparing the graphene nanoribbons such as plasma etching[67] and chemically derived techniques,[68] the BN nanoribbons may be prepared from the BN nanosheets. On the other hand, it is also possible to directly synthesize the BN nanoribbons by introducing catalysts[69] or using templates in our method. The present method to synthesize the BNNSs by CVD technique will undoubtedly provide new possibilities for preparing novel 2D BN materials.

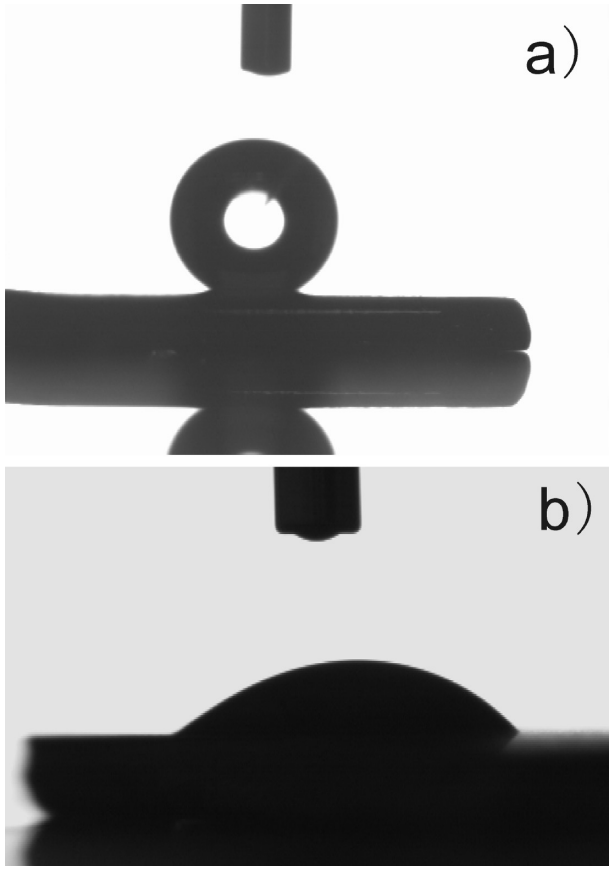

Figure 8. Typical photographs showing water droplets on the BNNF films (a) and granular BN films (b).

CONCLUSIONS

In summary, vertically aligned BNNSs were successfully synthesized by MPCVD on Si substrates from the gas mixtures of $BF_3-N_2-H_2$. The size, shape, and density of the BNNSs can be well-controlled by changing R_{H_2} and R_{BF_3} as well as their ratio, and the obtained BNNSs are as small as <5 nm in thickness. TEM images show that these BNNSs are cone-like with sharp open edges. Strong UV light emission and superhydrophobicity were achieved

for the BNNS films. The growth of the BNNSs is catalyst-free, which excludes the contamination from the catalysts, as occurred for growing carbon nanotubes, and increases the bonding strength with substrates. The present work opens a way to synthesize the 2D BN nanomaterials with controlled structures and demonstrates the application potential of the BNNSs in UV nanoelectronics and self-cleaning coatings.

METHODS

The growth of the BNNSs was performed in a quartz-tube-type MPCVD system. N-type (100) silicon monocrystal wafers were used as the substrates. The gas flow rates of N_2, H_2, and BF_3 (diluted in N_2 at 10%) are 150, 10−400, and 1−5 sccm, respectively. The purity of all the applied gases (purchased from Shenzhen Kaifeng Industrial Gas Co., Ltd., China) is 99.999%. The substrate temperature was about 800 °C, with the microwave power at 800 W and chamber pressure at 6 kPa during growth. SEM (HITACHI S-4700), TEM (JEM-2010), FTIR (NICOLET-380), and Raman spectroscopy (Renishaw RM-1000) were used to characterize the structures of the samples. EELS equipped in the TEM was used to determine the sample compositions. CL spectra were measured by using an Oxford Mono CL apparatus attached to the SEM system at room temperature. CA measurements were carried out by the sessile drop technique, where the water droplets were produced by a microsyringe and the angle of the liquid−solid interface was determined from the captured images.

Acknowledgment. This work was supported by the NSFC (Grant Nos. 50572019 and 50972033), New Century Excellent Talents in University (NCET060343), SRF for ROCS, SEM, and S&T Program of Shenzhen government.

REFERENCES AND NOTES

1. Novoselov, K. S.; Geim, A. K.; Morozov, S. V.; Jiang, D.; Zhang, Y.; Dubonos, S. V.; Grigorieva, I. V.; Firsov, A. A. Electric Field Effect in Atomically Thin Carbon Films. *Science* **2004**, *306*, 666–669.
2. Wu, Y. H.; Qiao, P. W.; Chong, T. C.; Shen, Z. X. Carbon Nanowalls Grown by Microwave Plasma Enhanced Chemical Vapor Deposition. *Adv. Mater.* **2002**, *14*, 64–67.
3. Shang, N. G.; Au, F. C. K.; Meng, X. M.; Lee, C. S.; Bello, I.; Lee, S. T. Uniform Carbon Nanoflake Films and Their Field Emissions. *Chem. Phys. Lett.* **2002**, *358*, 187–191.
4. Zhu, M. Y.; Wang, J. J.; Holloway, B. C.; Outlaw, R. A.; Zhao, X.; Hou, K.; Shutthanandan, V.; Manos, D. M. A Mechanism for Carbon Nanosheet Formation. *Carbon* **2007**, *45*, 2229–2234.
5. Shang, N. G.; Papakonstantinou, P.; McMullan, M.; Chu, M.; Stamboulis, A.; Potenza, A.; Dhesi, S. S.; Marchetto, H. Catalyst-Free Efficient Growth, Orientation and Biosensing Properties of Multilayer Graphene Nanoflake Films with Sharp Edge Planes. *Adv. Funct. Mater.* **2008**, *18*, 3506–3514.
6. Yu, A. P.; Ramesh, P.; Sun, X. B.; Bekyarova, E.; Itkis, M. E.; Haddon, R. C. Enhanced Thermal Conductivity in a Hybrid Graphite Nanoplatelet-Carbon Nanotube Filler for Epoxy Composites. *Adv. Mater.* **2008**, *20*, 4740–4744.
7. Wu, Y. H.; Yang, B. J.; Han, G. C.; Zong, B. Y.; Ni, H. Q.; Luo, P.; Chong, T. C.; Low, T.; Shen, Z. X. Fabrication of a Class of Nanostructured Materials Using Carbon Nanowalls as the Templates. *Adv. Funct. Mater.* **2002**, *12*, 489–494.
8. Yoo, E. J.; Kim, J.; Hosono, E.; Zhou, H. S.; Kudo, T.; Honma, I. Large Reversible Li Storage of Graphene Nanosheet Families for Use in Rechargeable Lithium Ion Batteries. *Nano Lett.* **2008**, *8*, 2277–2282.
9. Terrones, M.; Grobert, N.; Terrones, H. Synthetic Routes to Nanoscale $B_xC_yN_z$ Architectures. *Carbon* **2002**, *40*, 1665–1684.
10. Koi, N.; Oku, T.; Narita, I.; Suganuma, K. Synthesis of Huge Boron Nitride Cages. *Diamond Relat. Mater.* **2005**, *14*, 1190–1192.
11. Golberg, D.; Bando, Y.; Tang, C. C.; Zhi, C. Y. Boron Nitride Nanotubes. *Adv. Mater.* **2007**, *19*, 2413–2432.
12. Watanabe, K.; Taniguchi, T.; Kanda, H. Direct-Bandgap Properties and Evidence for Ultraviolet Lasing of Hexagonal Boron Nitride Single Crystal. *Nat. Mater.* **2004**, *3*, 404–409.
13. Paine, R. T.; Narula, C. K. Synthetic Routes to Boron Nitride. *Chem. Rev.* **1990**, *90*, 73–91.
14. Chen, Y.; Zou, J.; Campbell, S. J.; Caer, G. L. Boron Nitride Nanotubes: Pronounced Resistance to Oxidation. *Appl. Phys. Lett.* **2004**, *84*, 2430–2432.
15. Zhi, C. Y.; Bando, Y.; Tang, C. C.; Honda, S.; Sato, K.; Kuwahara, H.; Golberg, D. Characteristics of Boron Nitride Nanotube-Polyaniline Composites. *Angew. Chem., Int. Ed.* **2005**, *44*, 7929–7932.
16. Chopra, N. G.; Luyken, R. J.; Cherrey, K.; Crespi, V. H.; Cohen, M. L.; Louie, S. G.; Zettl, A. Boron Nitride Nanotubes. *Science* **1995**, *269*, 966–967.
17. Loiseau, A.; Willaime, F.; Demoncy, N.; Hug, G.; Pascard, H. Boron Nitride Nanotubes with Reduced Numbers of Layers Synthesized by Arc Discharge. *Phys. Rev. Lett.* **1996**, *76*, 4737–4740.
18. Terrones, M.; Hsu, W. K.; Terrones, H.; Zhang, J. P.; Ramos, S.; Hare, J. P.; Castillo, R.; Prassides, K.; Cheetham, A. K.; Kroto, H. W.; Walton, D. R. M. Metal Particle Catalysed Production of Nanoscale BN Structures. *Chem. Phys. Lett.* **1996**, *259*, 568–573.
19. Han, W. Q.; Bando, Y.; Kurashima, K.; Sato, T. Synthesis of Boron Nitride Nanotubes from Carbon Nanotubes by a Substitution Reaction. *Appl. Phys. Lett.* **1998**, *73*, 3085–3087.
20. Ma, R. Z.; Bando, Y.; Zhu, H. W.; Sato, T.; Xu, C. L.; Wu, D. H. Hydrogen Uptake in Boron Nitride Nanotubes at Room Temperature. *J. Am. Chem. Soc.* **2002**, *124*, 7672–7673.
21. Wang, J. S.; Kayastha, V. K.; Yap, Y. K.; Fan, Z. Y.; Lu, J. G.; Pan, Z. W.; Ivanov, I. N.; Puretzky, A. A.; Geohegan, D. B. Low Temperature Growth of Boron Nitride Nanotubes on Substrates. *Nano Lett.* **2005**, *5*, 2528–2532.
22. Chen, Z. G.; Zou, J.; Liu, Q. F.; Sun, C. H.; Liu, G.; Yao, X. D.; Li, F.; Wu, B.; Yuan, X. L.; Sekiguchi, T.; Cheng, H. M.; Lu, G. Q. Self-Assembly and Cathodoluminescence of Microbelts from Cu-Doped Boron Nitride Nanotubes. *ACS Nano* **2008**, *2*, 1523–1532.
23. Nakhmanson, S. M.; Calzolari, A.; Meunier, V.; Bernholc, J.; Nardelli, M. B. Spontaneous Polarization and Piezoelectricity in Boron Nitride Nanotubes. *Phys. Rev. B* **2003**, *67*, 235406-1–235406-5.
24. Blase, X.; Charlier, J. C.; Vita, A.; De; Car, R. Theory of Composite $B_xC_yN_z$ Nanotube Heterojunctions. *Appl. Phys. Lett.* **1997**, *70*, 197–199.
25. Choi, J.; Kim, Y. H.; Chang, K. J.; Tomanek, D. Itinerant Ferromagnetism in Heterostructured C/BN Nanotubes. *Phys. Rev. B* **2003**, *67*, 125421-1–125421-5.
26. Terrones, M.; Charlier, J. C.; Gloter, A.; Cruz-Silva, E.; Terres, E.; Li, Y. B.; Vinu, A.; Zanolli, Z.; Dominguez, J. M.; Terrones, H.; Bando, Y.; Golberg, D. Experimental and Theoretical Studies Suggesting the Possibility of Metallic Boron Nitride Edges in Porous Nanourchins. *Nano Lett.* **2008**, *8*, 1026–1032, and references therein.
27. Pacile, D.; Meyer, J. C.; Girit, C. O.; Zettl, A. The Two-Dimensional Phase of Boron Nitride: Few-Atomic-Layer Sheets and Suspended Membranes. *Appl. Phys. Lett.* **2008**, *92*, 133107-1–133107-3.
28. Han, W. Q.; Wu, L. J.; Zhu, Y. M.; Watanabe, K.; Taniguchi, T. Structure of Chemically Derived Mono- and Few-Atomic-Layer Boron Nitride Sheets. *Appl. Phys. Lett.* **2008**, *93*, 223103-1–223103-3.
29. Geick, R.; Perry, C. H.; Rupprecht, G. Normal Modes in Hexagonal Boron Nitride. *Phys. Rev.* **1966**, *146*, 543–547.

30. Nemanich, R. J.; Solin, S. A.; Martin, R. M. Light Scattering of Boron Nitride Microcrystals. *Phys. Rev.B* **1981**, *23*, 6348–6356.
31. Hoffman, D. M.; Doll, G. L.; Eklund, P. C. Optical Properties of Pyrolytic Boron Nitride in the Energy Range 0.05−10 eV. *Phys. Rev. B* **1984**, *30*, 6051–6056.
32. Wu, J.; Han, W. Q.; Walukiewicz, W.; Ager, J. W., III; Shan, W.; Haller, E. E.; Zettl, A. Raman Spectroscopy and Time-Resolved Photoluminescence of BN and $B_xC_yN_z$ Nanotubes. *Nano Lett.* **2004**, *4*, 647–650.
33. Kuzuba, T.; Eraa, K.; Ishii, T.; Sato, T. A Low Frequency Raman-Active Vibration of Hexagonal Boron Nitride. *Solid State Commun.* **1978**, *25*, 863–865.
34. Arenal, R.; Ferrari, A. C.; Reich, S.; Wirtz, L.; Mevellec, J. Y.; Lefrant, S.; Rubio, A.; Loiseau, A. Raman Spectroscopy of Single-Wall Boron Nitride Nanotubes. *Nano Lett.* **2006**, *6*, 1812–1816.
35. Moore, A. W. Compression Annealing of Pyrolytic Boron Nitride. *Nature* **1969**, *221*, 1133–1134.
36. Zhi, C. Y.; Bando, Y.; Tang, C. C.; Golberg, D.; Xie, R. G.; Sekigushi, T. Phonon Characteristics and Cathodoluminescence of Boron Nitride Nanotubes. *Appl. Phys. Lett.* **2005**, *86*, 213110-1–213110-3.
37. Saha, S.; Muthu, D. V. S.; Golberg, D.; Tang, C.; Zhi, C.; Bando, Y.; Sood, A. K. Comparative High Pressure Raman Study of Boron Nitride Nanotubes and Hexagonal Boron Nitride. *Chem. Phys. Lett.* **2006**, *421*, 86–90.
38. Yu, J.; Matsumoto, S. Synthesis of Thick and High Quality Cubic Boron Nitride Films by r.f. Bias Assisted d.c. Jet Plasma Chemical Vapor Deposition. *Diamond Relat. Mater.* **2004**, *13*, 1704–1708.
39. Chen, Z. G.; Zou, J.; Liu, G.; Li, F.; Wang, Y.; Wang, L. Z.; Yuan, X. L.; Sekiguchi, T.; Cheng, H. M.; Lu, G. Q. Novel Boron Nitride Hollow Nanoribbons. *ACS Nano* **2008**, *2*, 2183–2191.
40. Borowiak-Palen, E.; Pichler, T.; Fuentes, G. G.; Bendjemil, B.; Liu, X.; Graff, A.; Behr, G.; Kalenczuk, R. J.; Knupfer, M.; Fink, J. Infrared Response of Multiwalled Boron Nitride Nanotubes. *Chem. Commun.* **2003**, 82–83.
41. Andujar, J. L.; Bertran, E.; Maniette, Y. Microstructure of Highly Oriented, Hexagonal, Boron Nitride Thin Films Grown on Crystalline Silicon by Radio Frequency Plasma-Assisted Chemical Vapor Deposition. *J. Appl. Phys.* **1996**, *80*, 6553–6555.
42. Huang, J. L.; Pan, C. H.; Lii, D. F. Investigation of the BN Films Prepared by Low Pressure Chemical Vapor Deposition. *Surf. Coat. Technol.* **1999**, *122*, 166–175.
43. Choi, B. J. Chemical Vapor Deposition of Hexagonal Boron Nitride Films in the Reduced Pressure. *Mater. Res. Bull.* **1999**, *34*, 2215–2220.
44. El-Yadouni, A.; Soltani, A.; Boudrioua, A.; Thevenin, P.; Bath, A.; Loulergue, J. C. Investigation of the Optical and Electro-optical Properties of Hexagonal Boron Nitride Thin Films Deposited by PECVD Technique. *Opt. Mater.* **2001**, *17*, 319–322.
45. Kalss, W.; Haubner, R.; Lux, B. Preparation of BN Films in the B-N-F System. *Diamond Relat. Mater.* **1998**, *7*, 369–375.
46. Zhang, W. J.; Matsumoto, S. The Roles of Hydrogen and Fuorine in the Deposition of Cubic Boron Nitride Films in the Ar-N_2-BF_3-H_2 System. *Chem. Phys. Lett.* **2000**, *330*, 243–248.
47. Zhang, W. J.; Chan, C. Y.; Meng, X. M.; Fung, M. K.; Bello, I.; Lifshitz, Y.; Lee, S. T.; Jiang, X. The Mechanism of Chemical Vapor Deposition of Cubic Boron Nitride Films from Fluorine-Containing Species. *Angew. Chem., Int. Ed.* **2005**, *44*, 4749–4753.
48. Zhang, W. J.; Matsumoto, S. The Effects of dc Bias Voltage on the Crystal Size and Crystal Quality of cBN Films. *Appl. Phys. A: Mater. Sci. Process.* **2000**, *71*, 469–472.
49. Yu, J.; Zheng, Z.; Ong, H. C.; Wong, K. Y.; Matsumoto, S.; Lau, W. M. Thermal Stability of Cubic Boron Nitride Films Deposited by Chemical Vapor Deposition. *J. Phys. Chem. B* **2006**, *110*, 21073–21076.
50. Matsumoto, S.; Nishida, N.; Akashi, K.; Sugai, K. Preparation of BN Films by rf Thermal Plasma Chemical Vapour Deposition. *J. Mater. Sci.* **1996**, *31*, 713–720.
51. Mirkarimi, P. B.; McCarty, K. F.; Medlin, D. L. Review of Advances in Cubic Boron Nitride Film Synthesis. *Mater. Sci. Eng. R* **1997**, *21*, 47–100, and references therein.
52. Yu, J.; Zhang, Q.; Ahn, J.; Yoon, S. F.; Gan, B.; Chew, K.; Tan, K. H.; Bai, X. D.; Wang, E. G. Growth and Structure of Aligned B−C−N Nanotubes. *J. Vac. Sci. Technol. B* **2001**, *19*, 671–674.
53. Yu, J.; Ahn, J.; Yoon, S. F.; Zhang, Q.; Rusli; Gan, B.; Chew, K.; Yu, M. B.; Bai, X. D.; Wang, E. G. Semiconducting Boron Carbonitride Nanostructures: Nanotubes and Nanofibers. *Appl. Phys. Lett.* **2000**, *77*, 1949–1951.
54. Ural, A.; Li, Y. M.; Dai, H. J. Electric-Field-Aligned Growth of Single-Walled Carbon Nanotubes on Surfaces. *Appl. Phys. Lett.* **2002**, *81*, 3464–3466.
55. Wu, Y.; Yang, B. Effects of Localized Electric Field on the Growth of Carbon Nanowalls. *Nano Lett.* **2002**, *2*, 355–359.
56. Jaffrennou, P.; Barjon, J.; Lauret, J. S.; Attal-Tretout, B.; Ducastelle, F.; Loiseau, A. Origin of the Excitonic Recombinations in Hexagonal Boron Nitride by Spatially Resolved Cathodoluminescence Spectroscopy. *J. Appl. Phys.* **2007**, *102*, 116102-1–116102-3.
57. Silly, M. G.; Jaffrennou, P.; Barjon, J.; Lauret, J. S.; Ducastelle, F.; Loiseau, A.; Obraztsova, E.; Attal-Tretout, B.; Rosencher, E. Luminescence Properties of Hexagonal Boron Nitride: Cathodoluminescence and Photoluminescence Spectroscopy Measurements. *Phys. Rev. B* **2007**, *75*, 085205-1–085205-5.
58. Han, W. Q.; Yu, H. G.; Zhi, C.; Wang, J.; Liu, Z.; Sekiguchi, T.; Bando, Y. Isotope Effect on Band Gap and Radiative Transitions Properties of Boron Nitride Nanotubes. *Nano Lett.* **2008**, *8*, 491–494.
59. Feng, X. J.; Jiang, L. Design and Creation of Superwetting/Antiwetting Surfaces. *Adv. Mater.* **2006**, *18*, 3063–3078.
60. Yan, H.; Kurogi, K.; Mayama, H.; Tsujii, K. Environmentally Stable Super Water-Repellent Poly(alkylpyrrole) Films. *Angew. Chem., Int. Ed.* **2005**, *44*, 3453–3456.
61. Lau, K. K. S.; Bico, J.; Teo, K. B. K.; Chhowalla, M.; Amaratunga, G. A. J.; Milne, W. I.; McKinley, G. H.; Gleason, K. K. Superhydrophobic Carbon Nanotube Forests. *Nano Lett.* **2003**, *3*, 1701–1705.
62. Lee, C. H.; Drelich, J.; Yap, Y. K. Superhydrophobicity of Boron Nitride Nanotubes Grown on Silicon Substrates. *Langmuir* **2009**, *25*, 4853–4860.
63. Feng, X. J.; Zhai, J.; Jiang, L. The Fabrication and Switchable Superhydrophobicity of TiO_2 Nanorod Films. *Angew. Chem., Int. Ed.* **2005**, *44*, 5115–5118.
64. Bai, X. D.; Guo, J. D.; Yu, J.; Wang, E. G.; Yuan, J.; Zhou, W. Z. Synthesis and Field-Emission Behavior of Highly Oriented Boron Carbonitride Nanofibers. *Appl. Phys. Lett.* **2000**, *76*, 2624–2626.
65. Sugino, T; Kawasaki, S.; Tanioka, K.; Shirafuji, J. Electron Emission Characteristics of Boron Nitride Films Synthesized by Plasma-Assisted Chemical Vapor Deposition. *J. Vac. Sci. Technol., B* **1998**, *16*, 1211–1214.
66. Sugino, T.; Kimura, C.; Yamamoto, T. Electron Field Emission from Boron-Nitride Nanofilms. *Appl. Phys. Lett.* **2002**, *80*, 3602–3604.
67. Han, M. Y.; Ozyilmaz, B.; Zhang, Y. B.; Kim, P. Energy Band-Gap Engineering of Graphene Nanoribbons. *Phys. Rev. Lett.* **2007**, *98*, 206805-1–206805-4.
68. Li, X. L.; Wang, X. R.; Zhang, L.; Lee, S. W.; Dai, H. J. Chemically Derived, Ultrasmooth Graphene Nanoribbon Semiconductors. *Science* **2008**, *319*, 1229–1232.
69. Campos-Delgado, J.; Romo-Herrera, J. M.; Jia, X. T.; Cullen, D. A.; Muramatsu, H.; Kim, Y. A.; Hayashi, T.; Ren, Z. F.; Smith, D. J.; Okuno, Y.; Ohba, T.; Kanoh, H.; Kaneko, K.; Endo, M.; Terrones, H.; Dresselhaus, M. S.; Terrones, M. Bulk Production of a New Form of sp^2 Carbon: Crystalline Graphene Nanoribbons. *Nano Lett.* **2008**, *8*, 2773–2778.